ACS APPLIED MATERIALS & INTERFACES

Research Article

www.acsami.org

Two Orders of Magnitude Fluorescence Enhancement of Aluminum Phthalocyanines by Gold Nanocubes: A Remarkable Improvement for Cancer Cell Imaging and Detection

Yong-Kui Xu,[†] Sekyu Hwang,[‡] Sungjee Kim,[‡] and Ji-Yao Chen*[,†]

[†]State Key Laboratory of Surface Physics and Department of Physics, and Key Laboratory of Micro and Nano Photonic Structures (Ministry of Education), Fudan University, Shanghai 200433, China

[‡]Department of Chemistry, Pohang University of Science and Technology (POSTECH), San 31, Hyoja-Dong, Nam-Gu, Pohang, Gyeong-Buk, South Korea 790-784

ABSTRACT: The metal-enhanced fluorescence (MEF) by metal nanoparticles is a useful technique for fluorescence detections in biological systems. The MEF effects with gold nanorods (AuNRs) and nanocubes (AuNCs) for fluorescence enhancements of sulfonated aluminum phthalocyanine (AlPcS), a commonly used and clinical approved photosensitizer for photodynamic therapy of cancers, were studied in this work. For the AuNRs which have the low aspect ratios with the corresponding longitudinal surface plasma resonance (LSPR) band in the region of 600−750 nm, the fluorescence quenching of conjugated AlPcS was found. Whereas for the AuNRs that have the LSPR bands of 800−900 nm, the MEF of AlPcS was obtained with the enhancing factor of 2−6 times, respectively. Using AuNCs, a great enhancement of AlPcS fluorescence was achieved with an enhancing factor of 150 times. Using two cancer cell lines as in vitro models, an outstanding fluorescence enhancement of AlPcS-AuNCs conjugates in cells, relative to AlPcS alone, was obtained under one-photon excitation (OPE) of 405 nm. Moreover, the bright fluorescence image of AlPcS-AuNCs in cells was also achieved under the two-photon excitation (TPE) of an 800 nm femtosecond laser. The high-quality cell imaging with either OPE or TPE demonstrated the potential of AlPcS-AuNCs in cancer cell detections.

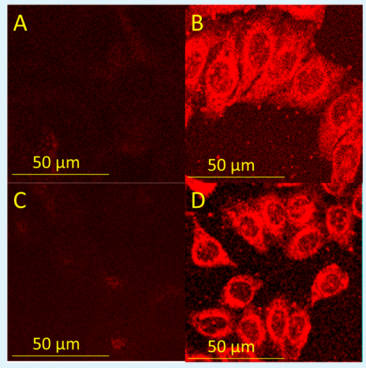

KEYWORDS: *metal-enhanced fluorescence, gold nanorods, gold nanocubes, surface plasma resonance, aluminum phthalocyanine*

1. INTRODUCTION

Fluorescence labeling has become a powerful tool in both clinical diagnosis[1,2] and basic biomedicine researches.[3,4] Although the techniques such as single photon counting have greatly increased the detection sensitivity, the fluorescence detection of probes in biological systems still meets the challenge of native fluorophore's autofluorescence in living body. If the probe's fluorescence intensity cannot surpass the autofluorescence, the signal/noise ratio (SNR) will be very poor. Increasing the SNR is still a hard task of fluorescence measurements in biological systems. The fluorescence lifetime imaging is a way to overcome the interference of autofluorescence, but this technique requires a long lifetime fluorescence probe to distinguish from the short lifetime (1−5 ns) fluorophores in living systems.[5] Metal enhanced fluorescence (MEF) is another approach developed recently.[6] Particularly, with the rapid development of nanotechnology the conjugates of the metal nanoparticles with fluorescent dyes have been tried for MEF, and these conjugates can be used as promising fluorescence probes in biomedical detections.[7−10] Because of the surface plasmon resonance (SPR) in metal nanoparticles, the electric field nearing the surfaces of nanoparticles is intensified[11] and the fluorescence quantum yield of attached fluorescent dye is increased because of the accelerated radiative rate by the SPR.[12] Therefore the fluorescence of surface-attached dyes can be enhanced. Among the metal nanoparticles, the gold nanoparticles (GNPs) have attracted much attention because of its chemical inertness and minimum biological toxicity.[13] In different structured GNPs, the gold nanorods (AuNRs) were the popular ones because of their two surface plasmon resonances (transverse and longitudinal, TSPR and LSPR) which are much stronger than that in gold spheres. Some tests with AuNRs have been reported for MEF.[10,14,15] However, only 1−3 times fluorescence enhancement by the AuNRs was found[16,17] and in some cases the quenched fluorescence of attached dyes on AuNRs was also reported.[18,19] In the MEF studies, the highest enhancement (7400-fold) was reported with the three-dimensional plasmonic nanoantenna-dots array grown on glass,[20] but these structures cannot be used as the probes in biological systems. Because of the strong SPRs covering the whole visible wavelength, the AuNRs have been expected to get strong enhancements but in fact no satisfactory results have been reached so far. This stimulated us to consider this problem and explore the possibility of using AuNRs to achieve a considerable MEF.

Received: January 7, 2014
Accepted: March 24, 2014
Published: March 24, 2014

   dx.doi.org/10.1021/am500106c | *ACS Appl. Mater. Interfaces* 2014, 6, 5619−5628

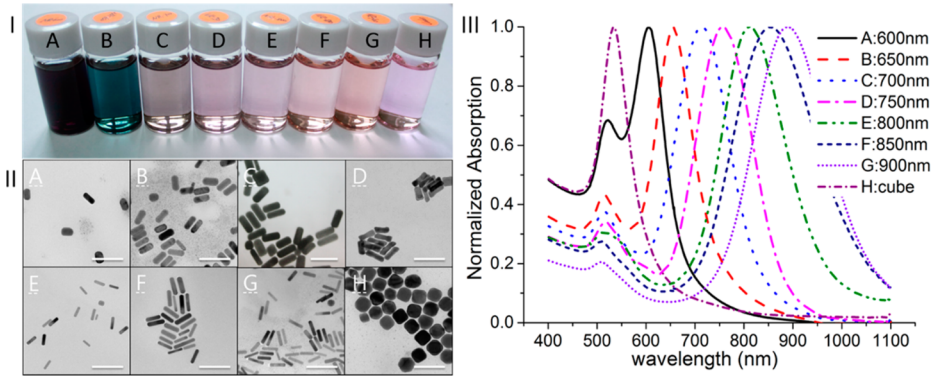

Figure 1. GNP characterization. (I) Picture of different gold nanoparticles in aqueous solutions, (II) their corresponding TEM images, and (III) extinction spectra. The samples of A to G are AuNRs with different aspect ratios, and the H is AuNCs. The scale bar in (II) is 100 nm.

In this work, the AuNRs with different aspect ratios were used to study the MEF effect and to investigate the interaction mechanism between the AuNRs and attached dyes. The sulfonated aluminum phthalocyanine (AlPcS), a popularly used and clinically approved photosensitizer for photodynamic therapy of cancers (PDT), was selected as the fluorescent dye for this MEF study. The fluorescence enhancement of AlPcS can benefit the cancer cell imaging and detection. In addition, the conjugates of AuNRs and AlPcS would facilitate their accumulation in tumors for further PDT applications, because the size of tens of nanometers of AuNRs fits well for the passive tumor accumulation due to the effect of enhanced permeability and retention (EPR) whereas the AlPcS itself is too small to retain in tumors effectively by this effect. Here we found that the energy transfer from excited AlPcS to the LSPR band of AuNRs is the main quenching effect of the AlPcS fluorescence and the mismatch between the excited state of AlPcS and LSPR of AuNRs by using the AuNRs with longer wavelength LSPR band can fulfill the MEF effect with an enhancing factor of 6 times. The gold nanocubes (AuNCs) only have a degenerate SPR so that they can get rid of this quenching effect. With the AuNCs, the AlPcS fluorescence was greatly enhanced with an enhancing factor of 150 times. To the best of our knowledge, this is the highest enhancing factor with GNPs. Moreover, the much brighter fluorescence images of conjugates of AlPcS-AuNCs in cancer cells were obtained relative to that of AlPcS under either one-photon excitation (OPE) or two-photon excitation (TPE), demonstrating its potential in PDT detections.

2. EXPERIMENTAL SECTION

2.1. Preparation of Gold Nanoparticles. According to the seeding growth method optimized previously,[21−24] the AuNRs with different aspect ratios were prepared. Followed by the addition of $HAuCl_4$ (20 mM, 125 μL) and CTAB (0.1 M, 7.5 mL) into a 10-mL glass bottle with gentle mixing, the $NaBH_4$ solution (10 mM, 0.6 mL), which was freshly prepared and ice-bathed, was then injected and magnetically stirred for about 2 min. When the color of the solution changed from yellow into brown, the 3.5 nm gold nanoseeds were obtained. The seed solution was then kept at 27 °C for at least 2 h before usage.

2.2. Growth of AuNRs and AuNCs. $HAuCl_4$ (20 mM, 250 μL) and $AgNO_3$ (10 mM, 0.1 mL) were mixed with CTAB (0.1 M, 10 mL) in a 20 mL glass tube with gentle mixing. Followed by the addition of ascorbic acid (0.1 M, 55 μL) the diluted gold seeds (120 μL) were injected into the growth solution, and left at 27 °C for overnight for the growth of AuNRs. By varying the molar ratio of $HAuCl_4$ to Silver nitrate, the AuNRs with different aspect ratios were prepared. The resulting aqueous solutions of gold nanorods with various aspect ratios were shown in figure 1(I). The AuNCs were prepared by mixing CTAB (0.1 M, 6.5 mL), HAuCl4 (20 mM, 0.4 mL), and ascorbic acid (0.1M, 3.8 mL) with 32 mL of deionized water in a 50 mL glass bottle before the 20 μL diluted seeds were injected. Had been gently mixed, the solution was left at 27 °C for overnight. Then the solution with pink color was shown in figure 1(I) H. These AuNRs and AuNCs were covered by the CTAB, so that they were positively charged dispersing well in aqueous solutions.

2.3. Characterization of Gold Nanoparticles. Absorption spectra of gold nanoparticles aqueous solutions were taken by Agilent 8453 UV−visible/NIR spectrophotometer using quartz cuvettes of 10 mm optical path length. The transmission electron microscopy (TEM) images were acquired in a JEM-2100 transmission electron microscope with the voltage of 200 kV. Zeta potential was measured in the Zetasizer Nano S90 with a standard 633 nm laser.

2.4. Preparation of Conjugates of AlPcS and Gold Nanoparticles. The AlPcS (frontier Scientific, Inc.) has the maximum four negative charges of the sulfonic groups on its four benzene rings. Therefore the AlPcS can easily bind on the surfaces of AuNRs or AuNCs by the electrostatic force to form conjugates. Mixing 5 μL of 1 mM AlPcS with 1 mL of 0.02nM AuNRs/AuNCs and stirring for overnight in the dark at 30 °C, the conjugates were formed. The sample solutions were then centrifuged at 8000g for 5 min to separate the conjugates and unconjugated free AlPcS in the supernatant. The harvested conjugates were resuspended in aqueous solution for the further experiments. In conjugation experiments, the different molar ratios between the AlPcS and AuNRs/AuNCs were tested to find the optimal one.

2.5. Cell Culture. Hela cells (human epithelial cervical cancer cell line) and KB cells (human nasopharyngeal epidermal carcinoma) were obtained from the cell bank of Shanghai Science Academy. Cells were maintained in DMEM medium with 10% calf serum, 100 units/mL penicillin, 100 ug/mL streptomycin and 100 ug/mL neomycin in a humidified standard incubator with a 5% CO_2 atmosphere at 37 °C. When the cells reached 80% confluence with normal morphology, the tested compound was added in and the cells were incubated in the incubator for 2 h for the case of conjugates of AuNCs-AlPcS or 24 h for free AlPcS, because the endocytosis process of the free AlPcS has been found to be very slow.[25] After incubation, these AlPcS or AlPcS-AuNCs incubated cells were washed three times with PBS (Phosphate-Buffered Saline) to remove unbound compounds and added with fresh medium. Then the cell samples were ready for fluorescence imaging measurements.

2.6. Fluorescence Measurements. The fluorescence spectra were measured in a spectrometer (Hitachi, F-2500). The fluorescence lifetime time was measured with the method of Time-Correlated Single Photon Counting (TCSPC). The TCSPC is based on the detection of single photons of a periodical light signal and the reconstruction of the waveform from the time measurements. A 2 × 10^7 Hz 405 nm picosecond (ps) laser (Edinburgh Instruments, EPL405) was employed for the excitation. The fluorescence decay

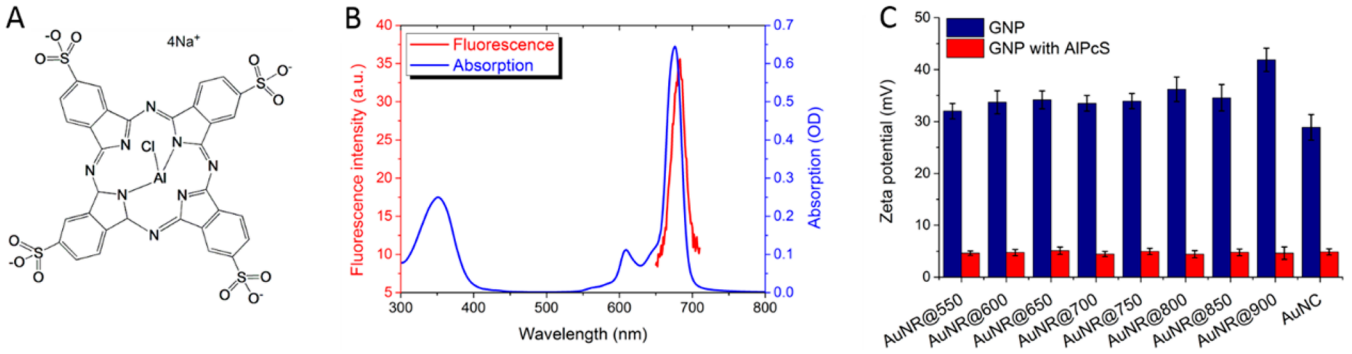

Figure 2. (A) Molecular structure of AlPcS; (B) the absorption and fluorescence spectra of AlPcS with concentration of 5 μM (excitation: 380 nm); (C) zeta potentials of GNPs and conjugates of AlPcS-GNPs.

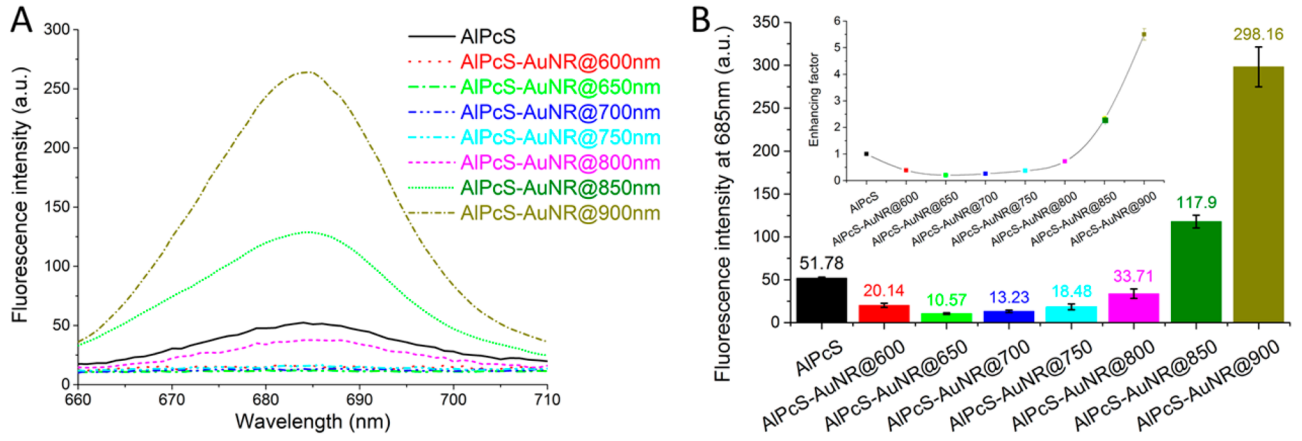

Figure 3. (A) Fluorescence spectra of different AlPcS-AuNRs in aqueous solutions and (B) the fluorescence intensities (at 685 nm) of each AlPcS-AuNRs relative to AlPcS. The LSPR wavelength of AuNRs represents its aspect ratio for each AuNRs.

courses were measured by a PMT (Hamamatsu, R928P) with a band-pass filter of 685 ± 15 nm in the TCSPC (Edinburgh Instruments, TCC900). The obtained decay curves can be fitted with multi-exponential decay as described in formula 1.

$$I(t) = \sum_{i=1}^{n} \alpha_i \exp\left(-\frac{t}{\tau_i}\right) \quad (1)$$

where τ_i and α_i represent the decay constant and amplitude of each exponential component, respectively. The average lifetime $\bar{\tau}$ can be obtained according to the formula 2

$$\bar{\tau} = \frac{\sum_{i=1}^{n} \alpha_i \tau_i^2}{\sum_{i=1}^{n} \alpha_i \tau_i} \quad (2)$$

With the numerous measurements, the average PL lifetimes in different cases were determined.

The fluorescence imaging of AlPcS in cells was acquired in a laser scanning confocal microscope (Olympus. FV300, IX 71) equipped with a matched pinhole and a band-pass filter of 685 nm in the detection channel. A water immersion objective (60×, NA = 1.2) was used in measurements. A 405 nm continuous laser was used for OPE imaging. Differential interference contrast (DIC) images were recorded simultaneously in a transmission channel to exhibit the cell morphology. For TPE imaging a near-infrared femtosecond (fs) laser (Mai Tai eHP DS) was coupled into the microscope to do excitation.

2.7. Cytotoxicity of AlPcS, AuNCs, and AlPcS-AuNCs. A new kind of MTT kit, the Cell Proliferation and Cytotoxicity Assay Kit (WST-1), was used to measure the cytotoxicity of AlPcS, AuNCs and the AlPcS-AuNCs on cells. Because AlPcS is a PDT (Photodynamic Therapy) drugs, light is strictly restricted during the treatment process. Two hundred microliters f cells with a concentration of 2×10^3 cells/mL were seeded in each well of a 96-well flat bottom tissue culture plat and allowed to attach to the plat for at least 8 h. When the cells reached 80% confluence with normal morphology, the culture medium with AlPcS (5 μM), AuNCs (50 pM), and AlPcS-AuNCs conjugates (5 μM-50pM) were added into different wells, respectively, and incubated for the desired time. Then, the cells were incubated in DMEM with 10 μL MTT solution (5 mg/mL) for another 2 h. Finally, the optical densities (O.D) at 450 nm of each well were measured in an iEMS Analyzer (Lab-system). The cell viability in each well was determined by comparing the O.D value with that of untreated control cells in wells of the same plate. All results were presented as the mean ± SE from three independent experiments with 6 wells in each.

3. RESULTS AND DISCUSSION

The as-prepared AuNRs and AuNCs were dispersed in aqueous solutions with different colors (Figure 1(I)) and their TEM images are shown in Figure 1(II). For the AuNRs, they have two SPR bands. The TSPR band locates about 530 nm, whereas the LSPR band is its aspect ratio dependent as the aspect ratio is bigger that the wavelength of LSPR is longer. Therefore we can use the wavelength of LSPR to mark the different AuNRs. Figure 1(III) gives the extinction spectra of these used AuNRs. Every AuNR has two extinction bands which correspond to its TSPR and LSPR. But the AuNC has a degenerate band around 540 nm.

The molecular structure of AlPcS is exhibited in Figure 2A and the absorption and fluorescence spectra are shown in Figure 2B. The AlPcS has two absorption bands located around 360 nm (B band) and 675 nm (Q-band), while its fluorescence band is at 685 nm. Since an AlPcS possesses 4 negative charges, it is easy to bind on the surface of positively charged GNPs to

dx.doi.org/10.1021/am500106c | ACS Appl. Mater. Interfaces 2014, 6, 5619−5628

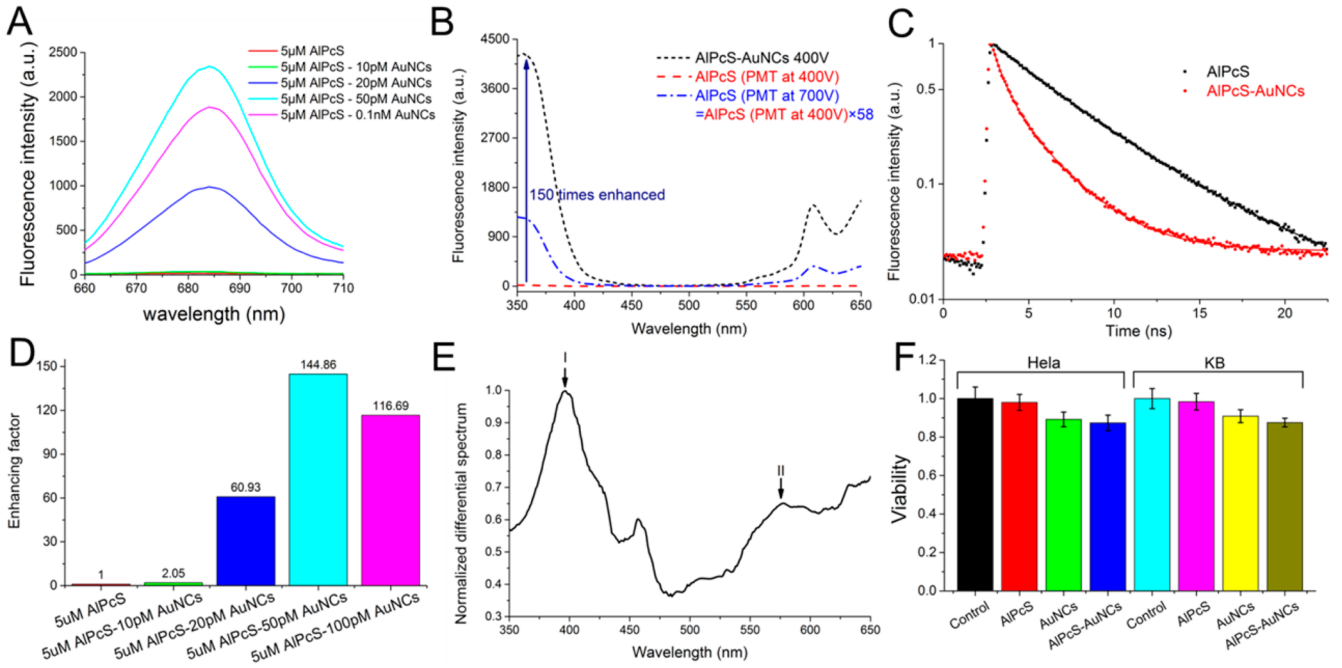

Figure 4. (A) Fluorescence emission spectra of AlPcS and AlPcS-AuNCs. Excitation: 380 nm. (B) The fluorescence excitation spectra of AlPcS (5 μM) and AlPcS-AuNCs (5 μM-50pM) at the emission wavelength of 685 nm. (C) Fluorescence lifetime decay curves of AlPcS and AlPcS-AuNCs. Excitation: 405 nm ps laser pulses. (D) Enhancing factor for each group AuNCs. (E) Differential spectrum made by AlPcS-AuNCs excitation spectrum divided by AlPcS excitation spectrum. (F) Cytotoxicities of used compounds on Hela and KB cells. The incubation concentration of AlPcS was 5 μM and that of AlPcS-AuNCs was 5 μM to 50 pM. The control groups were cells without any treatment of compounds.

form conjugates. This conjugation can be checked by the measurement of Zeta potential. When a molar ratio of 5 μM AlPcS to 50pM GNPs was selected to form the conjugates, the zeta potentials of GNPs and AlPcS-GNPs were measured, respectively, and shown in Figure 2C. The Zeta potentials of the AlPcS-GNPs decreased from +35 mV to +5 mV relative to unconjugated GNPs, indicating that AlPcS molecules have covered on the surfaces of GNPs confirming the successful conjugation of AlPcS and GNPs.

After the pre-examinations for different molar ratios, the 5 μM AlPcS to 50 pM AuNRs was used to form AlPcS-AuNRs for next MEF studies. The effects of aspect ratios of AuNRs on AlPcS fluorescence enhancement were comparatively measured and shown in Figure 3. The AlPcS fluorescence quenching was found for these AlPcS-AuNRs groups which have low aspect ratios, whereas the fluorescence enhancement was obviously seen for the AlPcS-AuNRs with the large aspect ratios, demonstrating that the aspect ratio of AuNRs played an important role on MEF.

The aspect ratio difference of these AuNRs is in fact the wavelength difference of their LSPR bands. As shown in Figure 1(III), the LSPR wavelength peaks of used AuNRs change from 600 to 900 nm. Noticing that the fluorescence band of AlPcS is centered at 685 nm but covered a wavelength region of about 80 nm, the overlapping of the AlPcS fluorescence band with the LSPR band of AuNRs could result in an energy transfer from AlPcS in the excited state to conjugated AuNRs quenching the AlPcS fluorescence. According to the fluorescence energy transfer theory, when the emission band of the donor is overlapped with the absorption band of the acceptor the energy transfer from the donor to acceptor occurs and the overlapping extent determines the transfer efficiency as the heavier the overlapping the higher the transfer efficiency.[26]

In previous MEF reports with AuNRs, several works found the quenched fluorescence and some others reported the enhanced fluorescence with an enhancing factor of about 1−3 times.[16,17] Now our result can give an explanation for this contradictory. Herein, the excited AlPcS on the surface of AuNRs could emit the fluorescence turning back to the ground state in one way or transfer the energy to conjugated AuNRs in another way when the LSPR lever of AuNRs matches the excited state of AlPcS. For the AuNRs groups with the LSPR bands from 600 to 750 nm, the overlapping extent of their LSPR with the AlPcS fluorescence band is serious so that the excited AlPcS would take de-excitation by transferring the energy to AuNRs resulting in a fluorescence quenching. But for the AuNRs with the LSPR bands of 850 and 900 nm, the fluorescence enhancements of conjugated AlPcS occurred with the enhancing factors of 2 and 6, respectively, because of the decrement of such overlapping. For all the AuNRs as shown in Figure 1(III), the long wavelength part of the TSPR band already extends to the short wavelength region of the LSPR band which makes AuNRs always have absorptions around 685 nm to some extents, so that the potential of using AuNRs to achieve a strong enhancement is very low. However, our results with AuNRs convinced the rule of energy transfer between the AlPcS and AuNRs, suggesting that the usage of other GNPs instead of AuNRs may increase the effect of MEF. Both gold nanospheres and AuNCs only have one SPR band around 540 nm so that no overlapping between the SPR level and the excited state of AlPcS exists, and thus the energy transfer from excited AlPcS to these GNPs can be avoided. Considering that the AuNCs have much stronger SPR relative to gold nanospheres,[27,28] the AuNCs were selected for further MEF studies.

The different molar ratios of AlPcS to AuNCs were arranged to search the best MEF of AlPcS-AuNCs. As shown in Figure

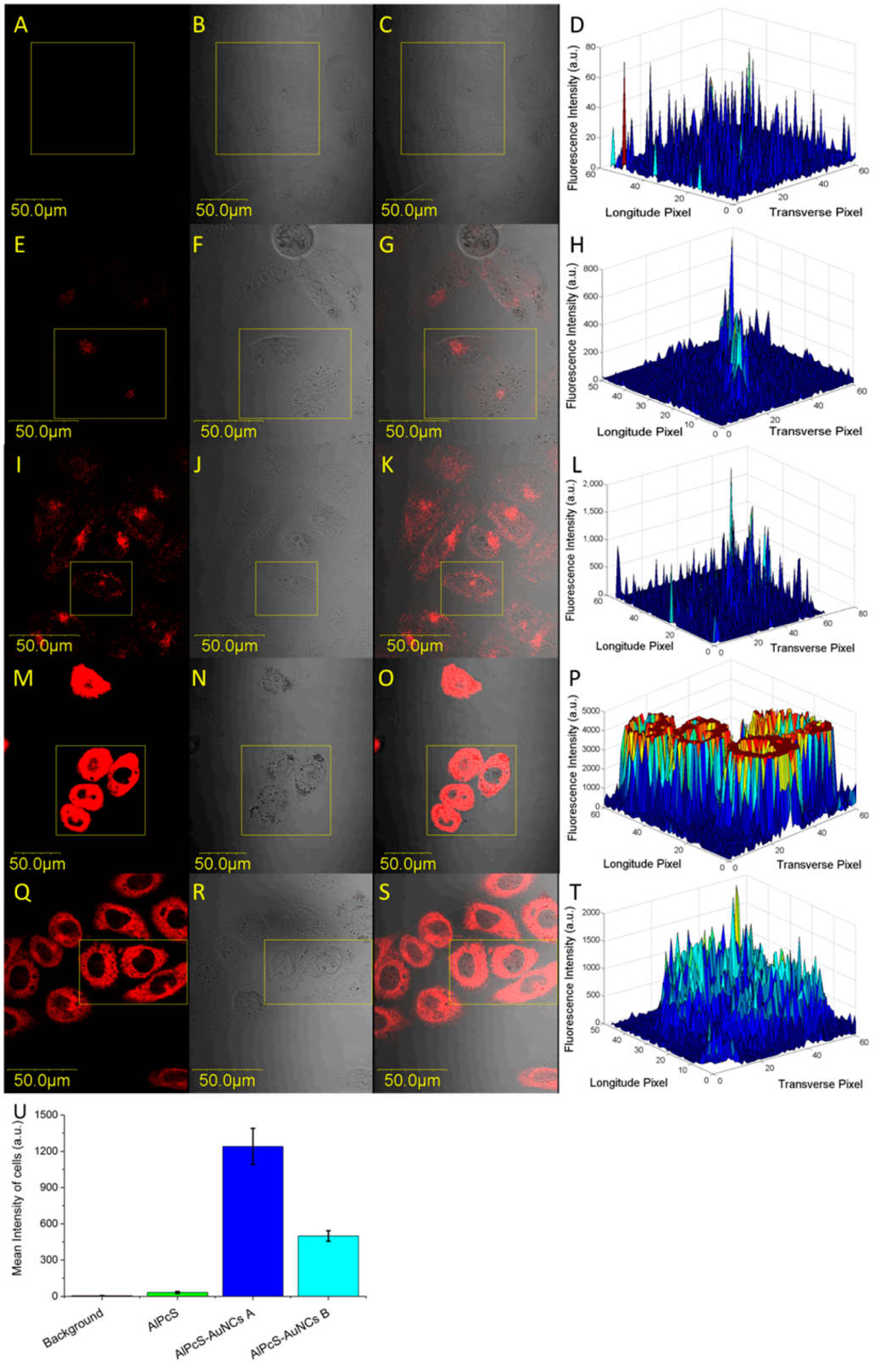

Figure 5. Fluorescence images of Hela cells (left column), DIC images (middle column), and merged images (right column). The first row is for control cells, the second and third rows are for AlPcS incubated cells under 5mW 405 nm OPE and measured at the PMT voltage of 720 and 850 V, respectively. The fourth and fifth rows are the fluorescence images of AlPcS-AuNCs incubated cells measured at PMT voltage of 720 V under 405 nm OPE with the power of 5 mW and a decreased power of 0.3 mW, respectively. The right insets (D, H, L, P and T) are the fluorescence intensity histograms in yellow rectangle framed areas of A, E, I, M, and Q of the figure, respectively. The U is a comparison of fluorescence imaging intensities of cellular AlPcS and AlPcS-AuNCs, measured in about 50 cells for each group at the same PMT voltage of 720 V. In U, the groups of AlPcS and AlPcS-AuNCs were measured under the excitation of 5 mW 405 nm, whereas the group of AlPcS-AuNCs B was measured with a decreased power of 0.3 mW.

dx.doi.org/10.1021/am500106c | ACS Appl. Mater. Interfaces 2014, 6, 5619−5628

4A, the AlPcS-AuNCs with a molar ratio of 1×10^5 (5 μM AlPcS to 50 pM AuNCs) can get an optimal fluorescence enhancement. The enhancing factor reaches 145 times (Figure 4D), which is one order magnitude higher than that of AlPcS-AuNRs. With the AuNCs, the breakthrough was achieved producing a highest enhancing factor for metal particle enhanced fluorescence. The fluorescence excitation spectra of AlPcS and AlPcS-AuNRs were measured (Figure 4B), and the differential spectrum made by AlPcS-AuNC excitation spectrum divided by AlPcS excitation spectrum was demonstrated in Figure 4E to show their difference. In Figure 4B, the fluorescence of AlPcS was too weak relative to that of AlPcS-AuNCs at the same detection PMT voltage of 400 V, so that the fluorescence excitation spectrum was additionally measured at the PMT voltage of 700 V. The PMT sensitivity at 700 V was 58 times higher than that at 400 V. The differential spectrum of Figure 4E can be used to study the interaction of AlPcS with AuNCs in AlPcS-AuNCs, in which two bands were seen with the wavelength around 390 and 560 nm. Comparing with the absorption spectrum of free AlPcS, the B band of conjugated AlPcS in fluorescence excitation spectrum was red-shifted (Figure 4B), resulting in a 390 nm differential band. The red-shift phenomenon has been commonly seen in two-bodies interaction as the energy levels of AlPcS were disturbed when being bound on the surfaces of AuNCs. This red-shift, on the contrary, confirms the close binding of AlPcS on the surfaces of AuNCs. The second differential band around 560 nm shows that the conjugated AlPcS can be excited at these wavelengths about 560 nm. The AlPcS itself has no absorption around 560 nm (Figure 2B), whereas the absorption band of AuNCs just locates in this region. Therefore, the fluorescence emission of conjugated AlPcS in AlPcS-AuNCs under the excitation of 560 nm can be deduced as the result of the energy transfer of AuNCs to AlPcS via the surface plasmon coupling.[29] The 560 nm differential band is another evidence of the interaction between the AlPcS and AuNCs.

The fluorescence lifetime change of AlPcS before and after binding on the AuNCs can further demonstrate the interaction of AlPcS and AuNCs in AlPcS-AuNCs. As shown in Figure 4C, the fluorescence lifetime of conjugated AlPcS in AlPcS-AuNCs is greatly shortened to 0.71 ns, whereas that of unconjugated AlPcS is 4.99 ns. On the basis of the MEF theory, the SPR in metal particles brings a new radiative rate Γ_m to attached fluorophores, and thus the emission quantum yield (Q_Y) is enhanced and the lifetime τ of the fluorophores is shortened, as described with the radiative rate τ and non- radiative rate in k_{nr} the following formulas.[30]

The emission quantum yield Q_Y is

$$Q_Y = \frac{\Gamma + \Gamma_m}{\Gamma + \Gamma_m + k_{nr}} \tag{3}$$

and the lifetime τ becomes

$$\tau = \frac{1}{\Gamma + \Gamma_m + k_{nr}} \tag{4}$$

Herein, the remarkably shortened fluorescence lifetime of conjugated AlPcS is consistent with the significant fluorescence enhancement. The obvious lifetime difference between the AlPcS-AuNCs and free AlPcS can be used to measure the controlled release of AlPcS from AlPcS-AuNCs, and we will carry out the releasing study in our next work.

The main difference between the AuNCs and AuNRs is that the AuNRs have two SPRs (TSPR and LSPR), whereas for the AuNCs their TSPR and LSPR combine together to become a degenerate SPR band around 540 nm. As shown in Figure 1, the LSPR bands for different aspect ratio AuNRs are all longer than 540 nm. When the LSPR band of AuNRs is overlapped with the emission band (centered at 685 nm) of AlPcS, the de-excitation of excited AlPcS can occur via energy transfer from excited AlPcS to AuNRs and thus quench the fluorescence of AlPcS, whereas for AuNCs, the unique SPR band locates at 540 nm, which differs much from the emission band of AlPcS (around 685 nm). Therefore, the quenching effect can be eliminated and the prominent fluorescence enhancement was achieved in AlPcS-AuNCs.

As fluorescence probes used in biomedical measurements, the toxicity is a great concern. The cytotoxicity of AlPcS-AuNCs was checked by the MTT assay on Hela and KB cells and compared with that of AlPcS and AuNCs. Figure 4F shows that the cytotoxicity of AlPcS-AuNCs is low. After incubation with AlPcS-AuNCs (5 μM-50pM) for 2 h, only a slight damage (about 10%) was found on cells. The low cytotoxicity of AlPcS-AuNCs benefits their further applications in biomedical field.

The 2 orders of magnitude fluorescence enhancement by AuNCs may greatly improve the cancer cell imaging and detection. The in vitro experiments were subsequently carried out to compare the fluorescence images of AlPcS and AlPcS-AuNCs.

For fair comparison, the cells were incubated with 5 μM AlPcS for 24 h and AlPcS-AuNCs (5 μM-50pM) for 2 h, respectively, because the cellular uptake of free AlPcS is slow. Images A, E, and M in Figure 5 give the fluorescence images of control cells, AlPcS-incubated cells, and AlPcS-AuNR-incubated cells, respectively, under the 5 mW 405 nm OPE and measured at the PMT voltage of 720 V, and panels D, H, and L in Figure 5 show their corresponding intensity histograms. The Figure 5E (AlPcS incubated cells) is too weak at the PMT voltage of 720 V, so that the PMT voltage of 850 V was used to increase the PMT sensitivity producing an observable fluorescence image of cellular AlPcS in Figure 5I. In contrast, the Figure 5M (AlPcS-AuNCs incubated cells) is so strong that the imaging intensity saturated. Then the fluorescence image of AlPcS-AuNCs incubated cells was remeasured with a decreased power of 0.3 mW of 405 nm laser and shown in Figure 5Q. For further comparison, the intensities of fluorescence images in about 50 cells in each case were quantitatively measured and calculated as shown in Figure 5U. The two-order magnitude fluorescence enhancement was also achieved in cell imaging by AlPcS-AuNCs.

The fluorescence enhancement of AlPcS-AuNCs on cell imaging was also demonstrated on another cancer cell line (KB cells). As shown in Figure 6, the MEF result of AlPcS-AuNCs in KB cells was obtained, consistent with that in Hela cells. Therefore, the AlPcS-AuNCs are suitable probes for cell imaging.

The fluorescence band of AlPcS is centered at 685 nm. For OPE of AlPcS, the excitation wavelength should be shorter than 685 nm. The optical window of living body is in the near-infrared (NIR) region of 700−900 nm,[31] and therefore the TPE with a NIR fs laser has become an attractive approach for PDT particularly for clinical applications of PDT. But the two-photon absorption cross-sections (TPACS) of commonly used photosensitizers including AlPcS were reported to be very low making the TPE ineffective.[32] The TPACS of AuNCs is also

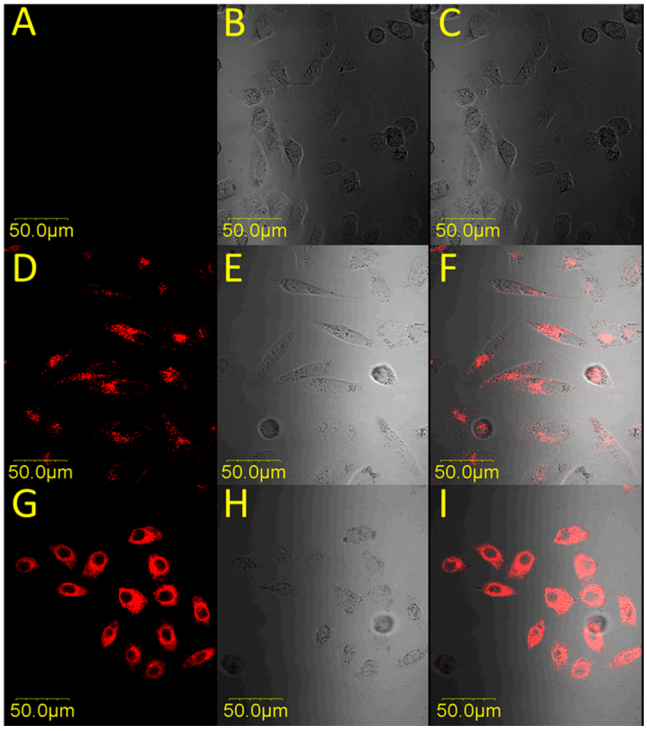

Figure 6. Fluorescence images of KB cells (left column), DIC images (middle column), and merged images (right column). The first row is for control cells, the second row is for AlPcS incubated cells measured at PMT of 850 V under 5 mW 405 nm OPE. The third row is for AlPcS-AuNCs incubated cells measured at PMT of 720 V under 405 nm OPE with the power of 0.3 mW.

not very high, which is 3 orders of magnitude lower than that of AuNRs.[29,33] However, the AlPcS-AuNCs can greatly enhance the fluorescence of conjugated AlPcS, so that the fluorescence imaging of cellular AlPcS-AuNCs under TPE of NIR fs laser became predictable. With TPE of an 800 nm fs laser, the fluorescence images of AlPcS and AlPcS-AuNCs loaded cells were measured, respectively, and shown in Figure 7. In contract to the blurred images of AlPcS loaded cells, the TPE images of AlPcS-AuNCs loaded cells are much brighter, demonstrating the potential of AlPcS-AuNCs in PDT detections with a NIR fs laser.

Because the AlPcS-AuNCs were prepared for biological applications, the stability of AlPcS-AuNCs, particularly their stability in physiological environments, was also a concerning problem. We selected the blood and cytoplasm as the physiological models to study the stability of AlPcS-AuNCs. When AlPcS and AlPcS-AuNCs were injected into human blood samples, respectively, the AlPcS fluorescence intensities were measured with the time for both AlPcS and AlPcS-AuNCs groups. As a clinically used drug, the AlPcS alone is extremely stable in blood since no fluorescence decrement can be found up to 24 h (Figure 8A). The stability of AlPcS-AuNCs is also good, as only a little decrement of their fluorescence intensity was found after 24 h in blood (Figure 8B). The stability of AlPcS-AuNCs in living cells was further studied in both Hela and KB cells. When cells have been incubated with AlPcS-AuNCs (5 μM to 50 pM) and washed with PBS and then added with fresh medium, the cell samples were put into incubators at 37 °C for a desired time period. The fluorescence images of cells were measured 2 and 24 h later, respectively, to check the stability of cellular AlPcS-AuNCs by observing the

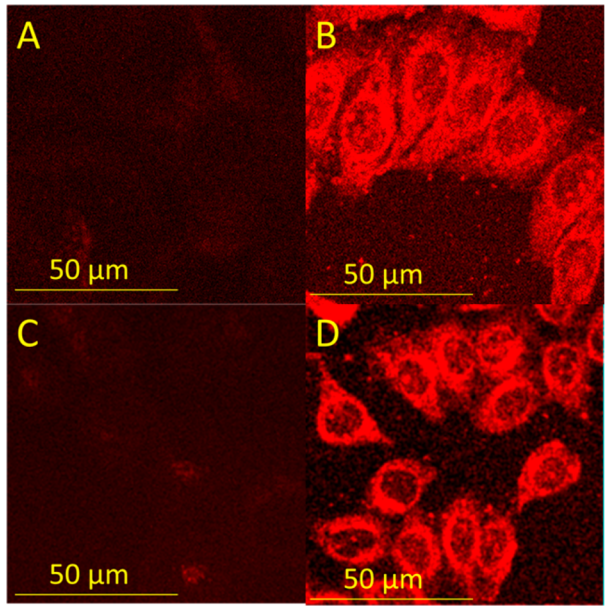

Figure 7. Fluorescence images of AlPcS or AlPcS-AuNCs in Hela and KB cells under the TPE of an 800 nm fs laser. The A and B are the images of AlPcS and AlPcS-AuNCs in Hela cells, respectively. The C and D are the images of AlPcS and AlPcS-AuNCs in KB cells, respectively. Cells have been incubated with AlPcS (5 μM) for 24 h or AlPcS-AuNCs (5 μM to 50 pM) for 2 h.

change of fluorescence images. As shown in Figure 8C–F, the AlPcS-AuNCs distribute in the cytoplasm of these two kinds of cells and this cellular distribution pattern does not change after 24 h. Moreover, the fluorescence imaging intensities of AlPcS-AuNCs in cells slightly decrease after 24 h incubation. Because the periods of cell division for these two cell lines are 16–20 h, the decrement of fluorescence imaging intensities of AlPcS-AuNCs after 24 h incubation may be partially due to the cell division. Therefore, the stability of cellular AlPcS-AuNCs is believed to be qualified. The good stability of AlPcS-AuNCs demonstrates its potential in biological applications.

The AlPcS-AuNCs achieved a 150 times fluorescence enhancement in water (Figure 4D). In fluorescence imaging measurements of AlPcS-AuNCs in cells (Figure 5), the enhancing ratio of AlPcS-AuNCs on fluorescence imaging as compared to the AlPcS alone was about 300 times (Figure 5U), which is obviously higher than that in water. The AlPcS is a negatively charged molecule so that the cell uptake rate is not high. The AuNCs are positively charged particles, and the z-potential of AlPcS-AuNCs is still +5 mV (Figure 2C). Therefore, the cell uptake rate of AlPcS-AuNCs could be high. The intracellular concentration of AlPcS or AlPcS-AuNCs is hard to determine, and thus the direct measurement of cell uptake is too difficult to reach. However, the relative compound amount in culture medium before and after incubation with cells can be measured by their fluorescence intensities. When cells were incubated with AlPcS or AlPcS-AuNCs, a part of the compound was taken up and the others were remained in the culture medium. The left compound amount in culture medium was measured by its fluorescence intensity and compared with that of the original compound amount. The fluorescence intensity decrement of AlPcS or AlPcS-AuNCs left in culture medium after cell incubation also can reflect the cell uptake rate. The cell uptake rate was thus determined by the following formula.

dx.doi.org/10.1021/am500106c | ACS Appl. Mater. Interfaces 2014, 6, 5619–5628

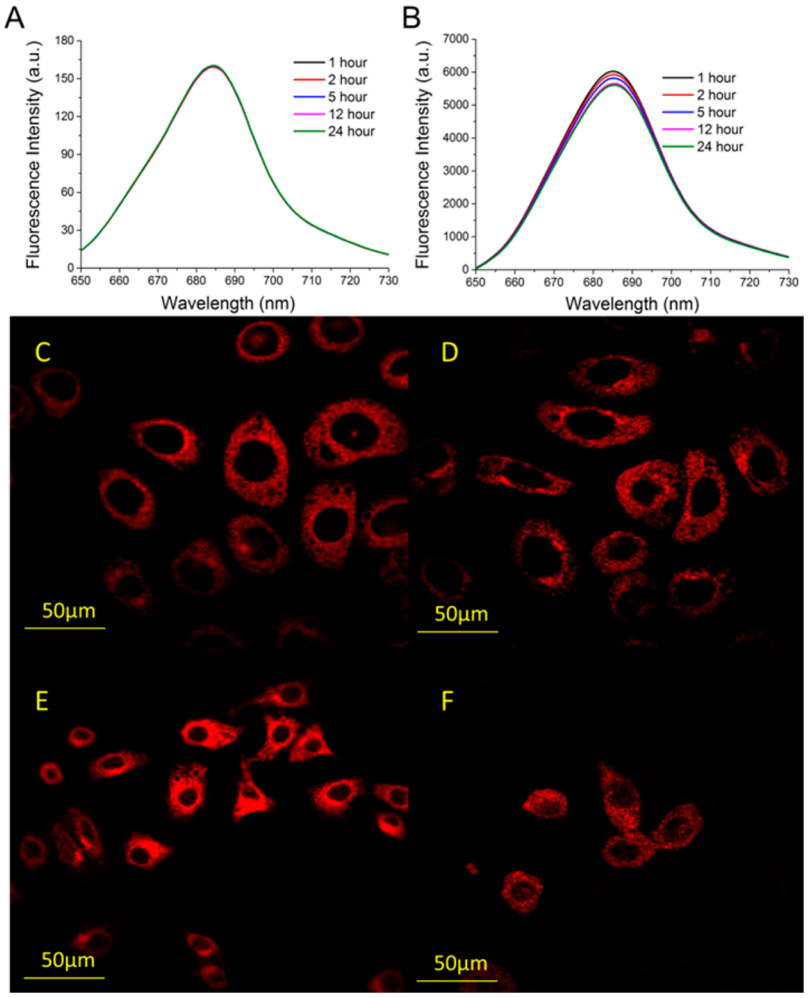

Figure 8. (B) Stability of AlPcS-AuNCs in human blood and living cells ((C, D) Hela cells and (E, F) KB cells). A and B are the fluorescence of AlPcS and AlPcS-AuNCs in human blood under 620 nm OPE, respectively. C and D are fluorescence images of AlPcS-AuNCs in Hela cells measured at 2 and 24 h after the AlPcS-AuNCs have been removed from the culture medium. E and F are that of KB cells. The fluorescence images were acquired by the PMT with the voltage of 720 V under 405 nm OPE with a power of 0.3 mW.

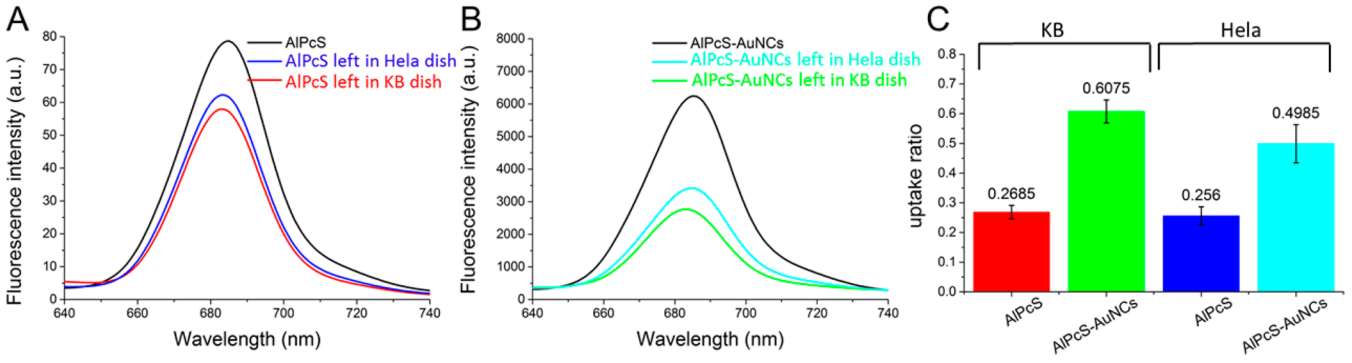

Figure 9. Cell uptake measurements of AlPcS and AlPcS-AuNCs by Hela and KB cells. (A) Fluorescence change of AlPcS in culture medium before and after 24 h incubation of cells. The original concentration of AlPcS was 5 μM dissolved in culture medium. The cells were cultured in the 3.5 cm diameter culture dish. (B) Fluorescence change of AlPcS-AuNCs in culture medium before and after 2 h incubation of cells. The original concentration of AlPcS-AuNCs was 5 μM to 50 pM. (C) Uptake rates of AlPcS and AlPcS-AuNCs by Hela and KB cells, calculated from the fluorescence change measured with more than 6 samples for each.

uptake rate = 1 − (fluorescence intensity of compound left in culture medium after cell incubation)/(fluorescence intensity of compound in culture medium before cell incubation)

According to this established method, the cell uptake rates of AlPcS and AlPcS-AuNCs for Hela and KB cells were measured, respectively, and shown in Figure 9. The cell uptake of AlPcS for both Hela and KB cells are similar with the uptake rates about 26%. The uptake rates of AlPcS-AuNCs by Hela and KB

dx.doi.org/10.1021/am500106c | ACS Appl. Mater. Interfaces 2014, 6, 5619−5628

cells reach 50−60%, which is two times higher than that of AlPcS. Summarizing the whole course of fluorescence enhancement on cell imaging, the AlPcS-AuNCs carry 2-fold drugs entering cells relative to AlPcS alone, and then perform the MEF in cells under the excitation producing an outstanding fluorescence enhancement on cell imaging.

4. CONCLUSION

In a fluorescence enhancement study of AlPcS with AuNRs, we found that the energy transfer from excited AlPcS to AuNRs is a key factor that seriously affects the efficiency of MEF. By using the AuNRs with the longer LSPR band which is unmatched to the energy level of excited AlPcS, the MEF in AlPcS-AuNRs can be obtained with the enhancing factor of 6. The AuNCs only have one degenerate and strong SPR band. The strong SPR in AuNCs produced an intensified electric field on the surfaces and accelerated the radiative rate of conjugated AlPcS also. In addition, in AlPcS-AuNCs there was no influence of LSPR involved energy transfer as that in AlPcS-AuNRs. Combining these beneficial factors together, the AlPcS-AuNCs fulfilled a remarkable fluorescence enhancement with an enhancing factor of 150. To the best of our knowledge, this is the highest fluorescence enhancement by metal nanoparticles so far. In previous reports, the enhancing factors by metal nanoparticles were all less than 10. This 2 orders of magnitude enhancement made AlPcS-AuNCs a powerful tool for cancer cell imaging which would facilitate the PDT detection. Particularly, the fluorescence images of AlPcS-AuNCs in cells was achieved by the TPE of a NIR fs laser demonstrating the potential in further in vivo applications, because the NIR lights have the best tissue penetration depths.

AUTHOR INFORMATION

Corresponding Author

*E-mail: jychen@fudan.edu.cn. Tel.: +86-21-65643084.

Notes

The authors declare no competing financial interest.

ACKNOWLEDGMENTS

Financial support from the National Natural Science Foundation of China (11074053 and 31170802) is gratefully acknowledged.

REFERENCES

(1) Cai, W.; Chen, K.; Li, Z.-B.; Gambhir, S. S.; Chen, X. Dual-Function Probe for PET and Near-Infrared Fluorescence Imaging of Tumor Vasculature. *J. Nucl. Med.* **2007**, *48* (11), 1862−1870.

(2) El-Sayed, M. A.; Shabaka, A. A.; El-Shabrawy, O. A.; Yassin, N. A.; Mahmoud, S. S.; El-Shenawy, S. M.; Al-Ashqar, E.; Eisa, W. H.; Farag, N. M.; El-Shaer, M. A.; Salah, N.; Al-Abd, A. M., Tissue Distribution and Efficacy of Gold Nanorods Coupled with Laser Induced Photoplasmonic Therapy in Ehrlich Carcinoma Solid Tumor Model. *Plos One* **2013**, *8* (10).

(3) Schuler, B.; Lipman, E. A.; Eaton, W. A. Probing the Tree-Energy Surface for Protein Folding with Single-Molecule Fluorescence Spectroscopy. *Nature* **2002**, *419* (6908), 743−747.

(4) Stryer, L. Fluorescence Spectroscopy of Proteins. *Science* **1968**, *162* (3853), 526−&.

(5) Berezin, M. Y.; Achilefu, S. Fluorescence Lifetime Measurements and Biological Imaging. *Chem. Rev.* **2010**, *110* (5), 2641−2684.

(6) Wokaun, A.; Lutz, H. P.; King, A. P.; Wild, U. P.; Ernst, R. R. Energy Transfer in Surface Enhanced Luminescence. *J. Chem. Phys.* **1983**, *79* (1), 509−514.

(7) Li, C. Y.; Zhu, J. F. Metal-Enhanced Fluorescence of OG-488 Doped in Au@SiO_2 Core−Shell Nanoparticles. *Mater. Lett.* **2013**, *112*, 169−172.

(8) Malicka, J.; Gryczynski, I.; Lakowicz, J. R. DNA Hybridization Assays Using Metal-Enhanced Fluorescence. *Biochem. Biophys. Res. Commun.* **2003**, *306* (1), 213−218.

(9) Chen, J.; Jin, Y. H.; Fahruddin, N.; Zhao, J. X. Development of Gold Nanoparticle-Enhanced Fluorescent Nanocomposites. *Langmuir* **2013**, *29* (5), 1584−1591.

(10) Li, X.; Kao, F. J.; Chuang, C. C.; He, S. L. Enhancing Fluorescence of Quantum Dots by Silica-Coated Gold Nanorods Under One- and Two-photon Excitation. *Opt. Express* **2010**, *18* (11), 11335−11346.

(11) Mishra, H.; Mali, B. L.; Karolin, J.; Dragan, A. I.; Geddes, C. D. Experimental and Theoretical Study of the Distance Dependence of Metal-Enhanced Fluorescence, Phosphorescence and Delayed fluorescence in a Single System. *Phys. Chem. Chem. Phys.* **2013**, *15* (45), 19538−44.

(12) Aslan, K.; Leonenko, Z.; Lakowicz, J. R.; Geddes, C. D. Annealed Silver-Island Films for Applications in Metal-Enhanced Fluorescence: Interpretation in Terms of Radiating Plasmons. *J. Fluoresc.* **2005**, *15* (5), 643−54.

(13) Zhang, W. Q.; Ji, Y. L.; Wu, X. C.; Xu, H. Y. Trafficking of Gold Nanorods in Breast Cancer Cells: Uptake, Lysosome Maturation, and Elimination. *ACS Appl. Mater. Interfaces* **2013**, *5* (19), 9856−9865.

(14) Fu, Y.; Zhang, J.; Lakowicz, J. R. Plasmon-Enhanced Fluorescence from Single Fluorophores End-Linked to Gold Nanorods. *J. Am. Chem. Soc.* **2010**, *132* (16), 5540−+.

(15) Kannan, P.; Rahim, F. A.; Chen, R.; Teng, X.; Huang, L.; Sun, H. D.; Kim, D. H. Au Nanorod Decoration on NaYF4:Yb/Tm Nanoparticles for Enhanced Emission and Wavelength-Dependent Biomolecular Sensing. *ACS Appl. Mater. Interfaces* **2013**, *5* (9), 3508−3513.

(16) Huang, X.; Tian, X. J.; Yang, W. L.; Ehrenberg, B.; Chen, J. Y. The Conjugates of Gold nanorods and Chlorin E6 for Enhancing the Fluorescence Detection and Photodynamic Therapy of Cancers. *Phys. Chem. Chem. Phys.* **2013**, *15* (38), 15727−15733.

(17) Gabudean, A. M.; Focsan, M.; Astilean, S. Gold Nanorods Performing as Dual-Modal Nanoprobes via Metal-Enhanced Fluorescence (MEF) and Surface-Enhanced Raman Scattering (SERS). *J. Phys. Chem. C* **2012**, *116* (22), 12240−12249.

(18) Li, X.; Qian, J.; Jiang, L.; He, S. L., Fluorescence Quenching of Quantum Dots by Gold Nanorods and Its Application to DNA Detection. *Appl. Phys. Lett.* **2009**, *94* (6).

(19) Wang, W. H.; Zhao, Y. N.; Jin, Y. Gold-Nanorod-Based Colorimetric and Fluorescent Approach for Sensitive and Specific Assay of Disease-Related Gene and Mutation. *ACS Appl. Mater. Interfaces* **2013**, *5* (22), 11741−11746.

(20) Zhou, L. C.; Ding, F.; Chen, H.; Ding, W.; Zhang, W. H.; Chou, S. Y. Enhancement of Immunoassay's Fluorescence and Detection Sensitivity Using Three-Dimensional Plasmonic Nano-Antenna-Dots Array. *Anal. Chem.* **2012**, *84* (10), 4489−4495.

(21) Mahmoud, M. A.; El-Sayed, M. A. Different Plasmon Sensing Behavior of Silver and Gold Nanorods. *J. Phys. Chem. Lett.* **2013**, *4* (9), 1541−1545.

(22) Eustis, S.; El-Sayed, M. Aspect Ratio Dependence of the Enhanced Fluorescence Intensity of Gold Nanorods: Experimental and simulation study. *J. Phys. Chem. B* **2005**, *109* (34), 16350−16356.

(23) Park, J. E.; Atobe, M.; Fuchigami, T. Synthesis of Multiple Shapes of Gold Nanoparticles with Controlled Sizes in Aqueous Solution Using Ultrasound. *Ultrason. Sonochem.* **2006**, *13* (3), 237−241.

(24) Ni, W.; Kou, X.; Yang, Z.; Wang, J. Tailoring Longitudinal Surface Plasmon Wavelengths, Scattering and Absorption Cross Sections of Gold Nanorods. *ACS Nano* **2008**, *2* (4), 677−686.

(25) Zhao, J. F.; Wang, J.; Chen, J. Y.; Chidawanykia, W.; Nyokong, T.; Ishii, K.; Kobayashi, N. Gallium Phthalocyanine Photosensitizers: Carboxylation Enhances the Cellular Uptake and Improves the

Photodynamic Therapy of Cancers. *Anti-Cancer Agents Med. Chem.* **2012**, *12* (6), 604−610.
(26) Medintz, I. L.; Clapp, A. R.; Mattoussi, H.; Goldman, E. R.; Fisher, B.; Mauro, J. M. Self-Assembled Nanoscale Biosensors Based on Quantum Dot FRET Donors. *Nat. Mater.* **2003**, *2* (9), 630−638.
(27) Chen, H. J.; Kou, X. S.; Yang, Z.; Ni, W. H.; Wang, J. F. Shape- and Size-Dependent Refractive Index Sensitivity of Gold Nanoparticles. *Langmuir* **2008**, *24* (10), 5233−5237.
(28) Kou, X. S.; Sun, Z. H.; Yang, Z.; Chen, H. J.; Wang, J. F. Curvature-Directed Assembly of Gold Nanocubes, Nanobranches, and Nanospheres. *Langmuir* **2009**, *25* (3), 1692−1698.
(29) Guan, Z. P.; Li, S.; Cheng, P. B. S.; Zhou, N.; Gao, N. Y.; Xu, Q. H. Band-Selective Coupling-Induced Enhancement of Two-Photon Photoluminescence in Gold Nanocubes and Its Application as Turn-on Fluorescent Probes for Cysteine and Glutathione. *ACS Appl. Mater. Interfaces* **2012**, *4* (10), 5711−5716.
(30) Deng, W.; Xie, F.; Baltar, H. T. M. C. M.; Goldys, E. M. Metal-enhanced Fluorescence in the Life Sciences: Here, Now and Beyond. *Phys. Chem. Chem. Phys.* **2013**, *15* (38), 15695−15708.
(31) Anderson, R. R.; Parrish, J. A. The Optics of Human-skin. *J. Invest. Dermatol.* **1981**, *77* (1), 13−19.
(32) Karotki, A.; Khurana, M.; Lepock, J. R.; Wilson, B. C. Simultaneous Two-Photon Excitation of Photofrin in Relation to Photodynamic Therapy. *Photochem. Photobiol.* **2006**, *82* (2), 443−452.
(33) Wu, X.; Ming, T.; Wang, X.; Wang, P. N.; Wang, J. F.; Chen, J. Y. High-Photoluminescence-Yield Gold Nanocubes: For Cell Imaging and Photothermal Therapy. *ACS Nano* **2010**, *4* (1), 113−120.